Interactions of fast ions with carbon nanotubes: Two-fluid model

D. J. Mowbray,[1] Z. L. Mišković,[1] F. O. Goodman,[1] and You-Nian Wang[2]
[1]*Department of Applied Mathematics, University of Waterloo, Waterloo, Ontario, Canada N2L 3G1*
[2]*The State Key Laboratory of Materials Modification by Beams, Department of Physics, Dalian University of Technology, Dalian 116023, People's Republic of China*
(Received 5 June 2004; published 15 November 2004)

We propose a simple, parameter-free two-fluid model for the collective electron response of a single-walled carbon nanotube, which treats the σ and π electrons as separate two-dimensional fluids constrained to the same cylindrical surface. The electrostatic interaction between the fluids gives rise to splitting of the plasmon frequencies into two groups closely following the experimentally determined longitudinal dispersions of the $\sigma+\pi$ and π plasmons. The model is used to calculate the induced electron density on the nanotube, as well as the stopping power for a charged particle moving parallel to the axis of the nanotube. It is found that these quantities exhibit novel features when the particle speed matches the phase velocity of the quasiacoustic π plasmon.

DOI: 10.1103/PhysRevB.70.195418 PACS number(s): 79.20.Rf, 34.50.Bw, 34.50.Dy

I. INTRODUCTION

Collective, or plasmon excitations of electrons on carbon nanotubes have been in the focus of intense experimental[1,2] and theoretical[3–11] research over the past several years. Such processes play an important role in a variety of recently studied interactions of charged particles with nanotubes, such as, screening of the charged impurities in the longitudinal direction,[12] channeling of ion or electron nanoscale beams through the nanotubes,[13–17] probing the nanotube response by the electron energy loss spectroscopy (EELS),[9,10] or formation of toroidal electron image states around nanotubes.[18,19] Ever since Ritchie's discovery of plasma oscillations in thin films,[20] the dielectric response formalism has been the most powerful theoretical tool for studying plasmon excitations in restricted geometries. For example, Arista has used recently this formalism to study the channeling of fast ions through nanocapillaries in solids,[21,22] as well as the plasmon excitations in cylindrical nanowires by external charged particles.[23] In addition, we have recently used an approach similar to Arista's work to evaluate the energy losses of fast ions moving inside the cylindrical tubules,[24] based on the dielectric function in random-phase approximation (RPA) for carbon nanotubes.[3,5]

Among various formulations of the dielectric response for nonhomogeneous electron systems, the hydrodynamic model has found a prominent place owing to its analytical simplicity and physical transparency, while retaining robustness in describing the main physical processes dominated by the plasmon excitations in many-electron systems.[6–9,25–28] Among different versions of the hydrodynamic model which are applicable to carbon nanotubes, the simplest one assumes that the electrons form a two-dimensional (2D) charged fluid confined to the cylindrical surface of a nanotube wall. Such a model has been used to calculate the plasmon spectra in multiwalled nanotubes (MWNT)[6] and, recently, to evaluate the energy losses of charged particles moving perpendicularly to a single-walled nanotube (SWNT),[9] as well as the self-energy and the stopping power of particles moving paraxially inside a SWNT.[25] To the credit of the hydrodynamic model, explicit comparisons were made in Ref. 25 showing that, as far as the energy losses and the self-energy of fast charges are concerned, the 2D hydrodynamic model gives the results which agree very well with those obtained from the dielectric-response formalism in RPA for a quasifree 2D electron gas.[5,24]

In the recent work on charged-particle interactions with SWNT,[9,25] the 2D electron fluid was assumed to consist of all four valence electrons per carbon atom, and it is appropriate to refer to it as the one-fluid model. This model was shown to give the resonant frequencies for the collective oscillations of the combined σ and π electron systems, commonly known as $\sigma+\pi$ plasmons,[1,2] whereas the lower frequencies, corresponding to the oscillations of the π electron system alone, were missing in the one-fluid model.[25] One way to remedy this situation is to treat the σ and π electron systems as two distinct but interacting 2D fluids confined to the same cylindrical surface of a nanotube. Such a two-fluid model was first developed by Barton and Eberlein (BE) to study the plasmon spectra in fullerenes,[27] and was subsequently applied to carbon nanotubes.[7] However, the BE two-fluid model contains adjustable parameters for plasmon frequencies which, although providing the necessary freedom in forcing the theoretical plasmon spectra to agree with experiments on carbon structures, are not always desirable in theoretical modeling.

We propose here a new, parameter-free version of the two-fluid model for a SWNT where the presence of internal interactions in each of the fluids enables the electrostatic coupling between the σ and π fluids to give rise to a splitting of the resonant excitation frequencies into two groups, which closely correspond to the experimentally identified branches of the high-frequency $\sigma+\pi$ plasmons and the low-frequency π plasmons.[1,2] Furthermore, we wish to investigate how the properties of this two-fluid model of a SWNT affect the stopping power of a point-charge particle channeled through the nanotube. In Sec. II we provide the basic equations for the two-fluid model, and in Sec. III we discuss the results of calculations of the induced electron density and the stopping power, which is followed by the concluding section.

Atomic units (a.u.) are used throughout, unless otherwise indicated.

II. BASIC THEORY

The development of the theory begins in a general form suitable for a MWNT consisting of N concentric cylinders, each with its own electron density,[6] but will be eventually specified to represent two fluids on one cylinder.

We use cylindrical coordinates $\mathbf{x}=\{r,\varphi,z\}$ for an arbitrary point in space, and define $\mathbf{x}_j=\{a_j,\varphi,z\}$ to represent the coordinates of a point on the cylindrical surface $r=a_j$ of the jth nanotube. Similarly, $\nabla_j=\hat{\mathbf{e}}_z(\partial/\partial_z)+a_j^{-1}\hat{\mathbf{e}}_\varphi(\partial/\partial_\varphi)$ differentiates only *tangentially* to the surface of the jth nanotube (with $1\leqslant j\leqslant N$). Let the perturbed state of the electron fluid on the jth nanotube be described by the electron number density per unit area, $n_j^0+n_j(\mathbf{x}_j,t)$, with n_j^0 being the unperturbed electron density on the jth nanotube, and by the velocity field, $\mathbf{u}_j(\mathbf{x}_j,t)$, which only has components tangential to the nanotube surface $r=a_j$. The linearized hydrodynamic model gives, for each j, the continuity equation for the induced density n_j,[25]

$$\frac{\partial n_j(\mathbf{x}_j,t)}{\partial t}+n_j^0\nabla_j\cdot\mathbf{u}_j(\mathbf{x}_j,t)=0, \tag{1}$$

and the momentum-balance equation,

$$\frac{\partial \mathbf{u}_j(\mathbf{x}_j,t)}{\partial t}=\nabla_j\Phi(\mathbf{x},t)|_{r=a_j}-\frac{\alpha_j}{n_j^0}\nabla_j n_j(\mathbf{x}_j,t)+\frac{\beta}{n_j^0}\nabla_j\left[\nabla_j^2 n_j(\mathbf{x}_j,t)\right]-\gamma_j\mathbf{u}_j(\mathbf{x}_j,t). \tag{2}$$

The first term on the right-hand-side of Eq. (2) is the force on an electron due to the tangential component of the electric field, evaluated at the nanotube surface $r=a_j$. The total electric potential, $\Phi=\Phi_{\text{ext}}+\Phi_{\text{ind}}$, is obtained from the Poisson equation in three dimensions (3D)[25] as the sum of the external potential and the induced potential due to the perturbations of the electron fluid densities on all nanotube surfaces,

$$\Phi_{\text{ind}}(\mathbf{x},t)=-\sum_l\int d^2\mathbf{x}_l'\frac{n_l(\mathbf{x}_l',t)}{\|\mathbf{x}-\mathbf{x}_l'\|}, \tag{3}$$

where $\mathbf{x}_l'=\{a_l,\varphi',z'\}$ and $d^2\mathbf{x}_l'=a_l\,d\varphi'\,dz'$ is the differential surface element on the lth nanotube. We note in passing that using Eq. (3) guarantees that the boundary conditions at all surfaces $r=a_j$ are automatically satisfied.[6,9,25] In that context, it is worthwhile mentioning that the present method of solving Eqs. (1)–(3), while being limited to the nanotubes placed in free space, is more direct than the usual approach based on undetermined coefficients which are fixed by enforcing the electrostatic boundary conditions.[6,7,9,25] The second term on the right-hand side of Eq. (2) is the force due to the internal interactions in the jth electron fluid, with $\alpha_j=\pi n_j^0$ being the square of the speed of propagation of the density disturbances in a 2D Fermi electron gas, whereas the third term with $\beta=1/4$ comes from the quantum correction for the kinetic energy in this gas and, as such, describes the onset of single-electron excitations in the fluid.[9,25] The last term in Eq. (2) represents the frictional force on an electron due to scattering on the positive-charge background, with γ_j being the friction coefficient, which we treat here as a (vanishingly) small constant.

By using the expansion of the Coulomb potential in cylindrical coordinates,[29]

$$\frac{1}{\|\mathbf{x}-\mathbf{x}'\|}=\sum_{m=-\infty}^{\infty}\int_{-\infty}^{\infty}\frac{dk}{(2\pi)^2}\times e^{ik(z-z')+im(\varphi-\varphi')}g(r,r';m,k), \tag{4}$$

where $g(r,r';m,k)\equiv 4\pi I_m(|k|r_<)K_m(|k|r_>)$ with $r_<=\min(r,r')$ and $r_>=\max(r,r')$, while I_m and K_m are cylindrical Bessel functions of integer order m, we are led to the definition of a Fourier-Bessel (FB) transform. So, with $\tilde{\Phi}(r,m,k,\omega)$ and $\tilde{n}_j(m,k,\omega)$ being the FB transforms of the potential (or any part of the potential) and the induced density, we can write, respectively,[25]

$$\Phi(\mathbf{x},t)=\sum_{m=-\infty}^{\infty}\int_{-\infty}^{\infty}\frac{dk}{(2\pi)^2}\int_{-\infty}^{\infty}\frac{d\omega}{2\pi}\times e^{ikz+im\varphi-i\omega t}\tilde{\Phi}(r,m,k,\omega), \tag{5}$$

$$n_j(\mathbf{x}_j,t)=\sum_{m=-\infty}^{\infty}\int_{-\infty}^{\infty}\frac{dk}{(2\pi)^2}\int_{-\infty}^{\infty}\frac{d\omega}{2\pi}\times e^{ikz+im\varphi-i\omega t}\tilde{n}_j(m,k,\omega). \tag{6}$$

By using Eqs. (4)–(6) in Eq. (3), one can express the FB transform of the induced potential as follows:

$$\tilde{\Phi}_{\text{ind}}(r,m,k,\omega)=-\sum_j g(r,a_j;m,k)a_j\tilde{n}_j(m,k,\omega). \tag{7}$$

In order to determine the FB transforms of the individual induced densities, $\tilde{n}_j$, we eliminate $\mathbf{u}_j$ from Eqs. (1) and (2), and use Eq. (7) along with the FB transform of the external potential, $\tilde{\Phi}_{\text{ext}}(r,m,k,\omega)$, to obtain the following set of coupled equations for $\tilde{n}_j$'s:

$$\left[\omega(\omega+i\gamma_j)-\alpha_j\left(k^2+\frac{m^2}{a_j^2}\right)-\beta\left(k^2+\frac{m^2}{a_j^2}\right)^2\right]\tilde{n}_j(m,k,\omega)-\sum_l G_{jl}(m,k)\tilde{n}_l(m,k,\omega)=-n_j^0\left(k^2+\frac{m^2}{a_j^2}\right)\tilde{\Phi}_{\text{ext}}(a_j,m,k,\omega), \tag{8}$$

where $G_{jl}(m,k) \equiv n_j^0 a_l[k^2+(m^2/a_j^2)]g(a_j,a_l;m,k)$.

In general, the set of equations (8) with $j=1,2,\ldots,N$ can be used to study a MWNT made of N concentric cylinders with $a_1<a_2<\cdots<a_N$ and with $n_1^0=n_2^0=\cdots=n_N^0\equiv n_0$, where $n_0=0.428$ is the unperturbed density per unit area of all valence electrons in the one-fluid approximation for each shell.[9,25] In that context, we note that, upon setting $\alpha_j=0$, $\beta=0$, $\gamma_j=0$, and $\Phi_{\text{ext}}=0$, Eq. (8) becomes identical to the eigenfrequency equation (13) in Ref. 6 for the resonant plasmon frequencies of a MWNT. However, in order to formulate our two-fluid model for a SWNT, we specify Eq. (8) to hold for $N=2$, and consider that the π fluid ($j=1$) and the σ fluid ($j=2$) reside on the same cylinder with radius $a_1=a_2\equiv a$, whereas $n_1^0\equiv n_\pi^0=n_0/4=0.107$ and $n_2^0\equiv n_\sigma^0=3n_0/4=0.321$ are the unperturbed densities per unit area corresponding to one π electron and three σ electrons per carbon atom, respectively. In this case, the resulting 2×2 matrix on the left-hand side of Eq. (8) gives the eigenvalue equation for the resonant frequencies of collective excitations in the two fluids, with the following two branches of the dispersion relations for each m:

$$\omega_\pm^2=\frac{\omega_\pi^2+\omega_\sigma^2}{2}\pm\sqrt{\left(\frac{\omega_\pi^2-\omega_\sigma^2}{2}\right)^2+\Delta^2}, \tag{9}$$

where $\omega_{\sigma,\pi}^2=\pi n_{\sigma,\pi}^0(k^2+m^2/a^2)+\frac{1}{4}(k^2+m^2/a^2)^2+n_{\sigma,\pi}^0 a(k^2+m^2/a^2)g(a,a;m,k)$ are the (squares of the) resonant frequencies of the individual σ and π electron fluids, and $\Delta=\sqrt{n_\sigma^0 n_\pi^0}a(k^2+m^2/a^2)g(a,a;m,k)$ describes the electrostatic interaction among the two fluids. We note at this point that the EB version of the two-fluid model,[27] as applied to SWNT,[7] is recovered by setting $\beta=0$ and $\gamma_j=0$, and by replacing the terms with the factors $\alpha_j=\pi n_j^0$ in Eqs. (8) and (9) by the squares of empirical resonant frequencies $\omega_{r\pi}^2$ and $\omega_{r\sigma}^2$ for the π and σ fluids. Given that the terms with α_j and β in our version of the two-fluid model contain the factors (k^2+m^2/a_j^2), we expect richer dispersion relations than those obtained in the EB version.[7] Let us also note here that the terms with β do not affect in any substantial way the low-m and the long-wavelength (small k) properties of the dispersion relations, Eq. (9), $\omega_+(m,k)$ and $\omega_-(m,k)$, but the presence of such terms guarantees that the electron response of the nanotube will be well defined for charged particles moving within the 2D electron fluid on the nanotube.[9,25]

III. RESULTS

A. Plasmon dispersion

Choosing the example of a SWNT with radius $a=7$ Å, we show in Fig. 1 the two groups of resonant plasmon dispersions from Eq. (9), $\omega_+(m,k)$ and $\omega_-(m,k)$, versus the longitudinal momentum k and for several angular modes $m=0$, 1, 2, 3, and 4, along with the experimental points from the EELS measurements of plasmon energies in bundles of SWNTs with the predominant values of radii being 7 Å.[1,2] The experimental configuration is certainly more complex than the present study of an isolated SWNT, so that the experimental data display some kind of an average over various

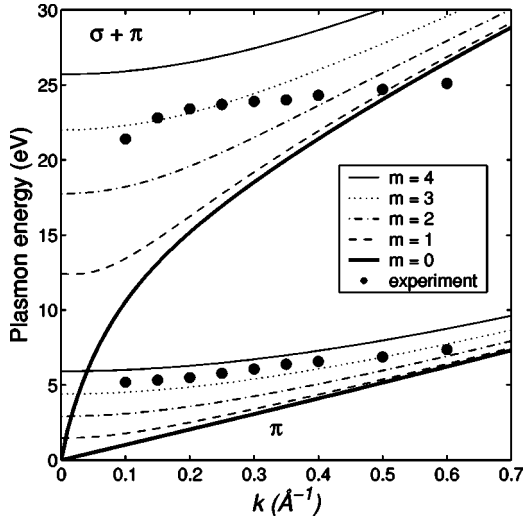

FIG. 1. Dispersion curves (in eV) $\omega_+(m,k)$ and $\omega_-(m,k)$ from Eq. (9), corresponding to the $\sigma+\pi$ and π plasmons in a nanotube with radius $a=7$ Å, shown versus longitudinal momentum k (in Å^{-1}) for several angular modes m. Experimental points are from Refs. 1 and 2.

(presumably lower valued) modes m. Nevertheless, those several dispersion curves, displayed in Fig. 1, show a good agreement with the experimental data, both in the magnitude and in the trend of the dispersion versus k. Given that the present two-fluid model is parameter-free, this agreement lends confidence in the proposed development of the hydrodynamic model.

It is apparent in Fig. 1 that the splitting between the two groups of plasmon frequencies in Eq. (9) is rather substantial owing to the strong electrostatic interaction between the σ and π fluids in the two-fluid model. Formally speaking, this splitting is strictly a consequence of the presence of the internal interactions in each fluid given by the terms in Eq. (2) with the factors α_j and β. To illustrate this point, we note that, if we set $\alpha_j=0$ and $\beta=0$ in Eq. (9), we find $\omega_-(m,k)=0$ and $\omega_+(m,k)=\omega_0(m,k)$, where $\omega_0^2=\pi n_0(k^2+m^2/a^2)+\frac{1}{4}(k^2+m^2/a^2)^2+n_0 a(k^2+m^2/a^2)g(a,a;m,k)$ defines the resonant frequencies ω_0 in the one-fluid model,[9,25] indicating that the σ and π fluids collapse into the combined $\sigma+\pi$ fluid in the absence of the internal interactions. When $\alpha_j\neq 0$ and $\beta\neq 0$ in Eq. (9), our calculations show that the dispersion curves $\omega_+(m,k)$ in the upper group in Fig. 1 are quite close to the corresponding one-fluid frequencies $\omega_0(m,k)$, so that this group is designated as the $\sigma+\pi$ plasmons. On the other hand, the dispersion curves $\omega_-(m,k,)$ are grouped in Fig. 1 around much lower energies, corresponding to the oscillations of the π electron fluid alone, and are thus called the π plasmons.[1,2] Moreover, while the $\sigma+\pi$ plasmon dispersions exhibit a characteristic dimensional crossover from a 2D to a one-dimensional electron system,[3,6] the π group of plasmon frequencies exhibits weaker dispersions. In particular, the $m=0$ mode in the π-plasmon group exhibits a remarkably linear dispersion for long wavelengths, which can be derived analytically in the form $\omega_-=k\sqrt{3\pi n_0/8}$. Given the prominence of the $m=0$ mode in various interaction configurations, it seems appropriate to call it quasiacoustic plasmon

mode. We note that a similar acoustic plasmon was discovered some time ago in the electron-hole plasma of a carbon nanotube.[4] In addition, another linear plasmon dispersion has been recently discovered in the coupling modes for two parallel nanotubes, and a possibility of the low-velocity drift instability of the electron plasma was discussed.[11] Reasoning along similar lines, we expect here that important effects will take place in the response of the two-electron fluid to a charged particle moving parallel to a SWNT at the speed v which closely matches the phase (and the group) velocity v_a of the acoustic plasmon in the two-fluid model, given by $v_a=\sqrt{3\pi n_0/8}=0.71$.

B. Induced electron density

We further study the induced electron density on the nanotube due to an external point charge Q moving on a paraxial trajectory $\mathbf{x}_0(t)=\{r_0,\varphi_0,vt\}$, so that $\tilde{\Phi}_{\rm ext}(r,m,k,\omega)=2\pi g(r,r_0;m,k)\delta(\omega-kv)\exp(-im\varphi_0)$. It should be noted that, owing to the translational invariance of the system in the z direction, both the induced density and the induced potential will be stationary in the moving frame of reference attached to the external charge. Choosing the external particle to be proton ($Q=1$) moving along the axis ($r_0=0$) of a SWNT with radius $a=7$ Å, we calculate the z dependence (in the moving frame) of the total induced electron density in the two-fluid model, $n_{\rm two}=n_\sigma+n_\pi$, and compare it in Figs. 2 and 3 with the induced density in the one-fluid model, $n_{\rm one}$, for a range of the particle speeds v. Because of the expected instabilities at $v\approx v_a$, we choose the friction coefficients to be small but finite parameters, $\gamma_\sigma=\gamma_\pi\equiv\gamma=10^{-3}\Omega_p$, with $\Omega_p=\sqrt{4\pi n_0/a}$ being a plasma frequency of a SWNT with the radius a.[24,25] Note that, because $r_0=0$, we have $\tilde{\Phi}_{\rm ext}(r,m,k,\omega)=8\pi^2\delta(\omega-kv)K_0(|k|r)\delta_{m,0}$, so that all contributions to the induced densities and the potential come from the $m=0$ terms in the FB series, Eq. (5) and (6). We also note that all curves shown in Figs. 2 and 3 have integrals over z which amount to $(2\pi a)^{-1}$, indicating that a complete screening of the external charge $Q=1$ takes place on the nanotube.

In the range of speeds above the threshold of about $v=2$ for the excitations of the $\sigma+\pi$ plasmons, one can observe in Fig. 2 that both $n_{\rm one}$ and $n_{\rm two}$ exhibit a development of the usual wake effect with increasing v, which manifests in the induced-density oscillations trailing the external charge ($z<0$). Apart from some minor differences in the periods and in the phases of these oscillations, the one-fluid and the two-fluid models give remarkably similar results for the speeds above $v=2$. On the other hand, for almost all v values in the low-speed range, $0<v<2$, our calculations show that $n_{\rm one}$ and $n_{\rm two}$ are practically on top of each other, just like in Fig. 2(a), both describing a symmetrical, bell-shaped accumulation of the electrons on the nanotube wall which screen the moving proton.

However, Fig. 3 shows careful inspection of a narrow range of the particle speeds around $v=0.71$ and reveals expected, yet qualitatively surprising differences in the z dependences of $n_{\rm one}$ and $n_{\rm two}$. Namely, while the one-fluid model maintains an almost rigidly shaped bell curve $n_{\rm one}(z)$, the two-fluid model gives rise to the development of a strong

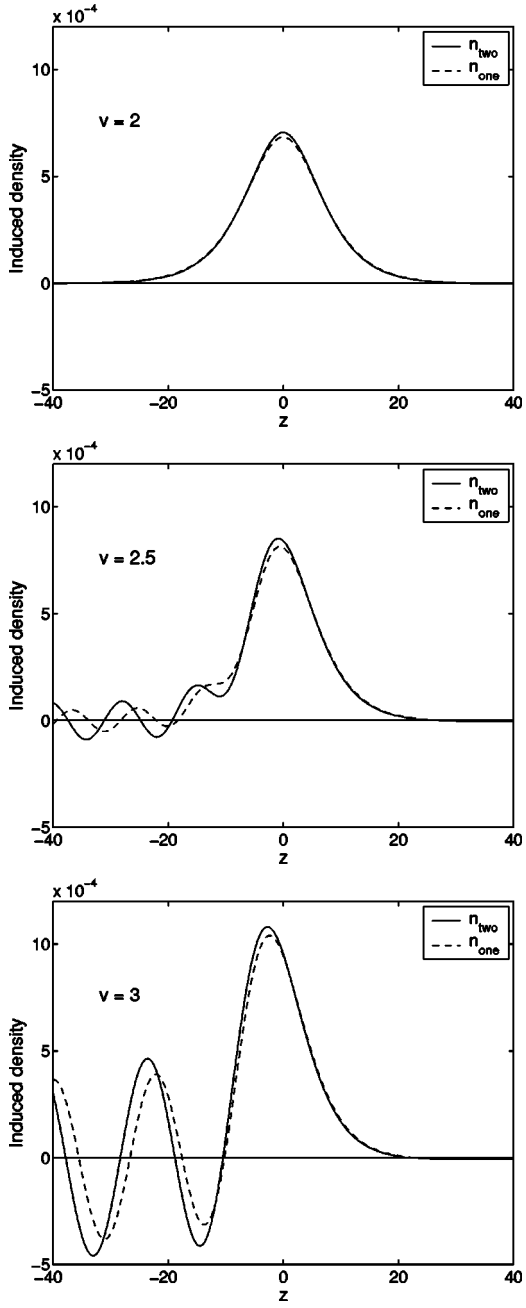

FIG. 2. Induced electron densities $n_{\rm one}$ and $n_{\rm two}$ (in a.u.) from the one-fluid and two-fluid models, versus distance z (in a.u.) in the moving frame of reference, for a proton moving along the axis of a nanotube with radius $a=7$ Å, at several speeds: $v=2$, 2.5, and 3 (a.u.).

asymmetry in the induced electron density $n_{\rm two}(z)$ in the range of speeds displayed in Fig. 3. The most surprising result is that $n_{\rm two}(z)$ exhibits oscillations for $v\approx 0.72$, shown in Fig. 3(b), which *precede* the external particle ($z>0$), in contrast to the trailing wake patterns shown in Figs. 2(b) and 2(c). Our calculations show that this physically puzzling behavior of the two-fluid model is accompanied by the strong, out-of-phase individual polarizations of the σ and π fluids, similar to the earlier observations in the electron-hole plasma on nanotubes.[4] We finally note that the calculations also

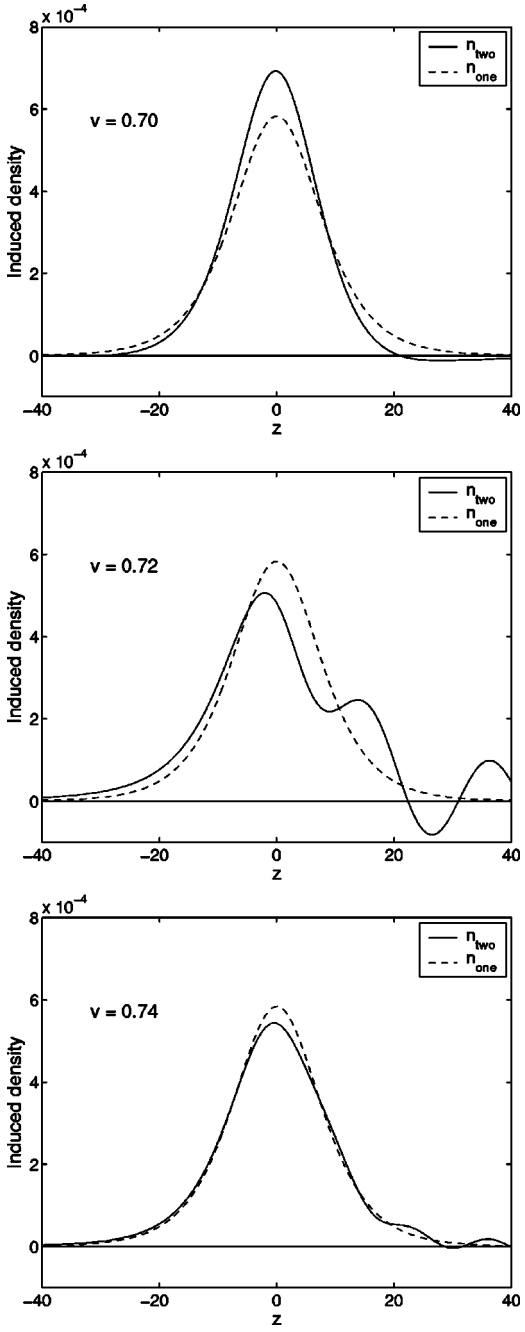

FIG. 3. Induced electron densities $n_{\rm one}$ and $n_{\rm two}$ (in a.u.) from the one-fluid and two-fluid models, versus distance z (in a.u.) in the moving frame of reference, for a proton moving along the axis of a nanotube with radius $a=7$ Å, at several speeds: $v=0.70$, 0.72, and 0.74 (a.u.).

show that, while both induced densities $n_{\rm one}$ and $n_{\rm two}$ are insensitive to the variations in (small) values of γ for high speeds, $v>2$, shown in Fig. 2, the oscillations in $n_{\rm two}$, shown in Fig. 3(b), are heavily damped when both the friction γ and the nanotube radius a increase.

C. Stopping power

Using the definition of the stopping power for a point charge Q moving parallel to the axis of a nanotube,

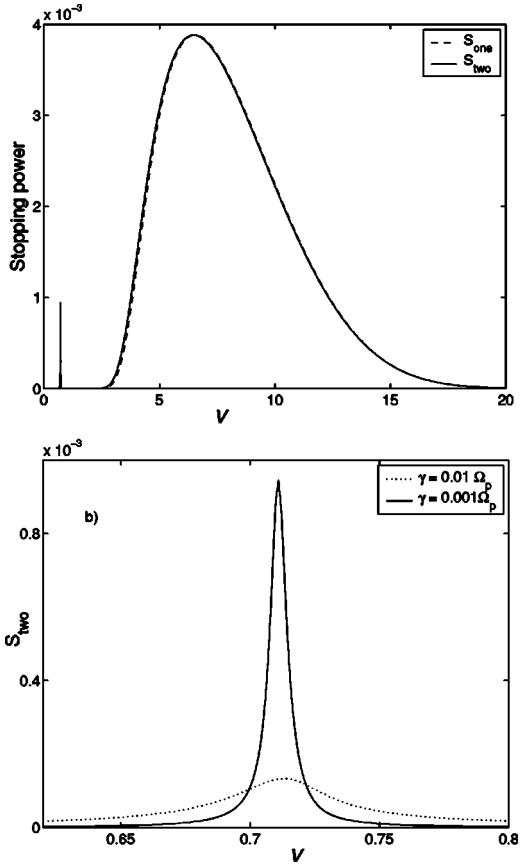

FIG. 4. Stopping power (in a.u.) versus speed v (in a.u.) for a proton moving along the axis of a nanotube with radius $a=7$ Å. (a) Stopping powers $S_{\rm one}$ and $S_{\rm two}$ (in a.u.) from the one-fluid and two-fluid models, with the friction constant $\gamma=10^{-3}\Omega_p$. (b) Stopping power $S_{\rm two}$ for two friction constants, $\gamma=10^{-3}\Omega_p$ and $\gamma=10^{-2}\Omega_p$.

$S=Q\partial\Phi_{\rm ind}/\partial_z|_{\mathbf{x}=\mathbf{x}_0(t)}$, we calculate the velocity dependences of the stopping powers $S_{\rm one}$ and $S_{\rm two}$ from the one-fluid and the two-fluid models, respectively. We first show in Fig. 4 the results for a proton moving along the axis ($r_0=0$) of a SWNT with radius $a=7$ Å, in which case only the $m=0$ modes contribute to both $S_{\rm one}$ and $S_{\rm two}$. In Fig. 4(a), we have used the friction coefficient $\gamma=10^{-3}\Omega_p$ and, not surprisingly, the two curves $S_{\rm one}$ and $S_{\rm two}$ are found to be almost on top of each other, except for a narrow peak in $S_{\rm two}$ at around $v=0.71$, which is absent in $S_{\rm one}$. It can be argued that the broad parts of both curves in Fig. 4(a) describe the excitation of the high-energy $\sigma+\pi$ plasmon with $m=0$ for speeds $v>2$, whereas the solitary peak in $S_{\rm two}$ describes the excitation of the low-energy acoustic π plasmon with $m=0$ when the proton speed matches its phase velocity $v_a=0.71$. As it was shown earlier for $S_{\rm one}$,[25] we have also verified here that the bulk parts of the stopping power curves for $v>2$ in Fig. 4(a) are insensitive to the variations in (small) values of γ. However, owing to the linear dispersion of the acoustic π plasmon with $m=0$, the peak structure at $v=0.71$ is quite sensitive to this variation, which is illustrated in Fig. 4(b) for two values of the friction constant, $\gamma=10^{-3}\Omega_p$ and $\gamma=10^{-2}\Omega_p$. These results suggest a possibility of having a drift instability at $v=v_a$,[11] which could provide a means of probing the collective electron excitations on the nanotubes, but they also

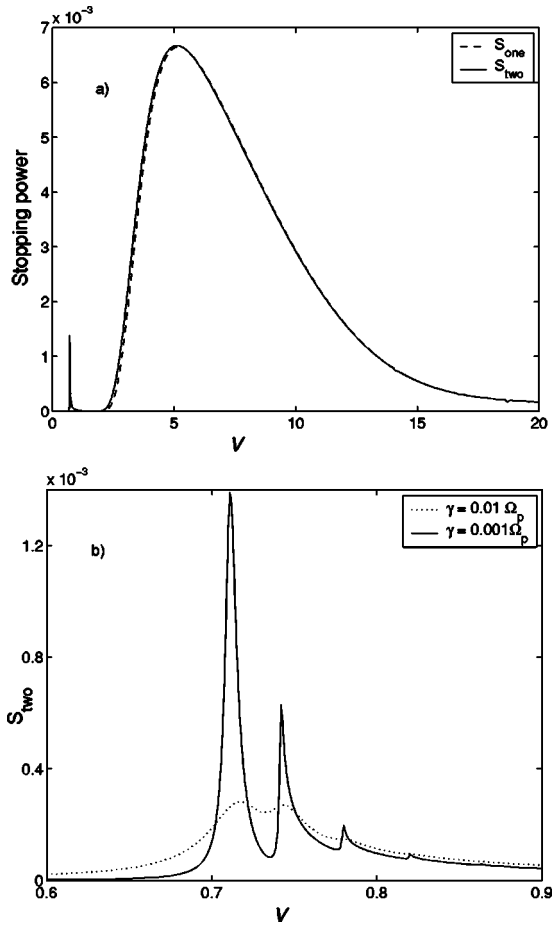

FIG. 5. Stopping power (in a.u.) versus speed v (in a.u.) for a proton moving at distance $r_0=a/2$ from the axis of a nanotube with radius $a=7$ Å. (a) Stopping powers S_{one} and S_{two} (in a.u.) from the one-fluid and two-fluid models, with the friction constant $\gamma=10^{-3}\Omega_p$. (b) Stopping power S_{two} for two friction constants, $\gamma=10^{-3}\Omega_p$ and $\gamma=10^{-2}\Omega_p$.

point to the need of a careful examination of the role of various damping mechanisms for the low-frequency plasmon modes.

Finally, in order to illustrate the effects of the plasmon excitations with $m\neq 0$ on the stopping power, we show in Fig. 5 the results for S_{one} and S_{two} for a proton moving at the distance $r_0=a/2$ from the axis of a SWNT with radius $a=7$ Å. Again, the two curves are on top of each other in Fig. 5(a) for the speeds v above the threshold for the $\sigma+\pi$ plasmon excitations, and they both closely reproduce the data obtained earlier, including those based on the dielectric function in RPA.[25] In the low-speed region, S_{two} displays multiple peaks, which are shown in Fig. 5(b) for $\gamma=10^{-3}\Omega_p$ and $\gamma=10^{-2}\Omega_p$, exhibiting the sensitivity of these peaks to damping. For the smaller γ value, one can easily identify in Fig. 5(b) several peaks corresponding to the excitations of the π plasmons with $m=0$, 1, 2, and 3, in a nice correspondence with the π plasmon dispersion curves shown in Fig. 1.

IV. CONCLUDING REMARKS

We have proposed a simple, parameter-free version of the two-fluid model for the hydrodynamic response of the electrons on a SWNT, which treats the σ and π electrons as separate 2D charged fluids constrained to the same cylindrical surface. The strong electrostatic interaction between the fluids gives rise to the splitting of the collective-excitation frequencies into two sets which closely follow the experimental dispersion curves for the high-energy $\sigma+\pi$ plasmons and the low-energy π plasmons. In particular, the $m=0$ mode of the π plasmons exhibits a quasiacoustic, linear dispersion versus the longitudinal wave number. Calculations of the induced electron density on the nanotube and the stopping power for a charged particle moving parallel to the nanotube axis show that, at the particle speeds above the threshold for the $\sigma+\pi$ plasmon excitations, the two-fluid model essentially follows the results of the one-fluid model, whereas the range of low particle speeds reveals some effects due to the π plasmon excitations in the two-fluid model. In particular, when the particle speed matches the phase velocity of the acoustic π plasmon, the induced density shows oscillations which precede the position of the particle, in contrast to the usual wake oscillations, whereas the speed dependence of the stopping power of the particle displays peaked structures around that phase velocity. It has been found that, while the high-speed stopping power is insensitive to the friction coefficient, the low-speed peaks are quite dependent on it. This finding points to a need to further improve the proposed two-fluid model by carefully examining the role of damping at lower plasmon frequencies.

While the present work uses the linearized version of hydrodynamic model, it is important to consider the nonlinear effects in future developments. In that context, the existing 3D and 2D nonlinear approaches for low velocities may provide a background for important future comparison.[30,31] On the other hand, implementation of the two-fluid model into a future quasiparticle-lifetime investigation might give contribution to understanding electron excitations in graphite-based nanostructures.[32,33]

ACKNOWLEDGMENTS

This work was supported by the Natural Sciences and Engineering Research Council of Canada. One of the authors (Z.L.M.) acknowledges support by PREA. One of the authors (Y.-N.W.) acknowledges support by the National Natural Science Foundation of China.

[1] T. Pichler, M. Knupfer, M.S. Golden, J. Fink, A. Rinzler, and R.E. Smalley, Phys. Rev. Lett. **80**, 4729 (1998).
[2] M. Knupfer, T. Pichler, M.S. Golden, J. Fink, A. Rinzler, and R.E. Smalley, Carbon **37**, 733 (1999).
[3] M.F. Lin and K.W.-K. Shung, Phys. Rev. B **47**, 6617 (1993).
[4] O. Sato, M. Kobayashi, Y. Tanaka, and A. Hasegawa, Phys. Rev. B **52**, 4677 (1995).
[5] M.F. Lin, D.S. Chuu, C.S. Huang, Y.K. Lin, and K.W.-K. Shung, Phys. Rev. B **53**, 15 493 (1996).
[6] C. Yannouleas, E.N. Bogachek, and U. Landman, Phys. Rev. B **53**, 10 225 (1996).
[7] X. Jiang, Phys. Rev. B **54**, 13 487 (1996).
[8] B. Vasvári, Phys. Rev. B **55**, 7993 (1997).
[9] T. Stöckli, J.M. Bonard, A. Châtelain, Z.L. Wang, and P. Stadelmann, Phys. Rev. B **64**, 115424 (2001).
[10] D. Taverna, M. Kociak, V. Charbois, and L. Henrard, Phys. Rev. B **66**, 235419 (2002).
[11] G. Gumbs and A. Balassis, Phys. Rev. B **68**, 075405 (2003).
[12] K. Sasaki, Phys. Rev. B **65**, 195412 (2002).
[13] L.A. Gevorgian, K.A. Ispirian, and R.K. Ispirian, Nucl. Instrum. Methods Phys. Res. B **145**, 155 (1998).
[14] G.V. Dedkov and B.S. Karamurzov, Surf. Coat. Technol. **128–129**, 51 (2000).
[15] N.K. Zhevago and V.I. Glebov, Phys. Lett. A **310**, 301 (2003).
[16] S. Bellucci, V.M. Biryukov, Yu.A. Chesnokov, V. Guidi, and W. Scandale, Nucl. Instrum. Methods Phys. Res. B **202**, 236 (2003).
[17] A.A. Greenenko and N.F. Shul'ga, Nucl. Instrum. Methods Phys. Res. B **205**, 767 (2003).
[18] B.E. Granger, P. Král, H.R. Sadeghpour, and M. Shapiro, Phys. Rev. Lett. **89**, 135506 (2002).
[19] D. Segal, P. Král, and M. Shapiro, Phys. Rev. B **69**, 153405 (2004).
[20] R.H. Ritchie, Phys. Rev. **106**, 874 (1957).
[21] N.R. Arista and M.A. Fuentes, Phys. Rev. B **63**, 165401 (2001).
[22] N.R. Arista, Phys. Rev. A **64**, 032901 (2001).
[23] J.L. Gervasoni and N.R. Arista, Phys. Rev. B **68**, 235302 (2003).
[24] Y.-N. Wang and Z.L. Mišković, Phys. Rev. A **66**, 042904 (2002).
[25] Y.-N. Wang and Z.L. Mišković, Phys. Rev. A **69**, 022901 (2004).
[26] G. Barton, Rep. Prog. Phys. **42**, 65 (1979).
[27] G. Barton and C. Eberlein, J. Chem. Phys. **95**, 1521 (1991).
[28] E. Prodan and P. Nordlander, J. Chem. Phys. **120**, 5444 (2004).
[29] J.D. Jackson, *Classical Electrodynamics* (Wiley, New York, 1975).
[30] I. Nagy, A. Arnau, P.M. Echenique, and E. Zaremba, Phys. Rev. B **40**, 11 983 (1989).
[31] E. Zaremba, I. Nagy, and P.M. Echenique, Phys. Rev. Lett. **90**, 046801 (2003).
[32] C.D. Spataru, M.A. Cazalilla, A. Rubio, L.X. Benedict, P.M. Echenique, and S.G. Louie, Phys. Rev. Lett. **87**, 246405 (2001).
[33] G. Moos, C. Gahl, R. Fasel, M. Wolf, and T. Hertel, Phys. Rev. Lett. **87**, 267402 (2001).